HYDRODYNAMIC SOLVER FOR A TRANSIENT, TWO-FLUID, THREE-FIELD MODEL ON UNSTRUCTURED GRIDS

J.J. Jeong,[*1] H.Y. Yoon,[2] J. Kim,[1] I.K. Park[2] and H.K. Cho[2]

비정렬격자계에서 과도 이상유동해석을 위한 수치해법

정 재 준,[*1] 윤 한 영,[2] 김 종 태,[1] 박 익 규,[2] 조 형 규[2]

A three-dimensional (3D) unstructured hydrodynamic solver for transient two-phase flows has been developed for a 3D component of a nuclear system code and a component-scale analysis tool. A two-fluid three-field model is used for the two-phase flows. The three fields represent a continuous liquid, an entrained liquid, and a vapour field. An unstructured grid is adopted for realistic simulations of the flows in a complicated geometry. The semi-implicit ICE (Implicit Continuous-fluid Eulerian) numerical scheme has been applied to the unstructured non-staggered grid. This paper presents the numerical method and the preliminary results of the calculations. The results show that the modified numerical scheme is robust and predicts the phase change and the flow transitions due to boiling and flashing very well.

Key Words : A Transient Two-fluid Three-field Model, Unstructured Grid, Semi-implicit ICE Scheme

1. INTRODUCTION

A realistic simulation of two-phase flows is essential for the design and safe operation of a nuclear reactor system. The state-of-the-art nuclear system analysis codes, such as RELAP5-3D[1], TRAC-PF1[2], CATHARE2[3], MARS[4], etc., use one-dimensional two-fluid models for the analysis of transient two-phase flows in light water nuclear reactors. All the flows are assumed to take place in one-dimensional ducts and are described with their cross-sectional-average parameters such as void fraction, enthalpy, etc. However there are some situations, e.g., flows in the downcomer of a pressurized water reactor, flows through the steam generator tube bundles, etc., that are clearly three-dimensional[5].

These have motivated the development of 3D thermal-hydraulic components for the above-mentioned system codes. The 3D components, however, adopt a structured grid based on rectangular Cartesian or cylindrical coordinates. Therefore a realistic modeling of the flow in a complicated geometry is inherently difficult and, thus, a proper geometry input modeling is needed. These limitations can be covered in part by using the so-called component-scale analysis codes, such as FLICA[6], ATHOS[7], GOTHIC[8], etc. However, since these have been developed for component-specific uses, either fluid models for two-phase flows or numerical solution schemes are not appropriate for general transient two-phase flows in complicated flow geometries.

The use of CFD (computational fluid dynamics) codes for a detailed analysis of two-phase flows in a nuclear reactor coolant system[9] has also been extensively studied and it is known to be very promising. But, the capabilities of the CFD codes are currently restricted to certain two-phase flow regimes and, furthermore, they require a huge computational cost[10]. It seems that the direct use of two-phase CFD codes for a system transient analysis would not be practical for a few decades. In recognition

접수일: 2007년 9월 18일, 심사완료일: 2007년 11월 6일.
1 정회원, 한국원자력연구원
2 한국원자력연구원
* Corresponding author, E-mail: jjjeong@kaeri.re.kr

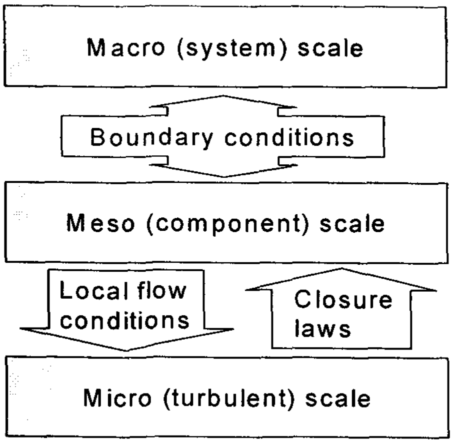

Fig. 1 The concept of multi-scale computations[11].

of this, the concept of a "multi-scale" analysis has been developed[11,12]. The behavior of an entire system is obtained by using a system code. Local phenomena in a part of a system may be addressed at the meso-scale (component scale) level, with the relevant tools considering smaller scales and more detailed flow models. Finally, one may need to obtain wall and interfacial momentum, heat, and mass transfer laws by performing studies at the smallest possible scale. Figure 1 shows the concept of a multi-scale analysis.

The primary objective of this work is to develop an unstructured hydrodynamic solver that can be used for both the 3D component of a system code and component-scale analysis tools. In this work, a transient, three-dimensional, two-fluid, three-field model is adopted and the governing equations are solved on an unstructured mesh, which is very useful for flows in a complicated geometry. As for the numerical solution scheme, the semi-implicit ICE method[1,13,14] has been modified for an unstructured non-staggered grid. This paper presents the numerical method for the unstructured hydrodynamic solver and the preliminary results of the calculations.

2. Governing Equations of the Two-Fluid Three-Field Model

A transient two-fluid three-field model was adopted for two-phase flows. In this model, the three fields represent a continuous liquid, an entrained liquid(droplet), and a vapor field[4]. The use of the three-field model is particularly useful in describing the thermal-hydraulics of a nuclear reactor and containment during a hypothetical large-break loss of coolant accident. The mass, energy, and momentum equations for each field are established separately and, then, they are linked by the interfacial mass, energy, and momentum transfer models. The resulting governing equations are similar to those of the time-averaged two-fluid equations derived by Ishii and Hibiki[15].

The continuity equation is

$$\frac{\partial}{\partial t}(\alpha_k \rho_k) + \nabla \cdot (\alpha_k \rho_k \underline{u}_k) = \Gamma_k \tag{1}$$

where k=l, d, v(continuous liquid, entrained liquid, vapor)

α: volume fraction,

ρ: density,

$\underline{u}$: velocity,

Γ_k: interfacial mass transfer rate per volume.

The momentum equation is given by

$$\frac{\partial}{\partial t}(\alpha_k \rho_k \underline{u}_k) + \nabla \cdot (\alpha_k \rho_k \underline{u}_k \underline{u}_k) = -\alpha_k \nabla P + \nabla \cdot [\alpha_k (\tau_k + \tau_k^T)] + \alpha_k \rho_k \underline{g} + \underline{u}_{ki} \Gamma_k + \underline{M}_{ik} - \nabla \alpha_k \cdot \tau_{ki} \tag{2}$$

where P: pressure,

u_{ki}: interface velocity of k-phase,

τ_k: viscous shear stress,

τ_k^T: turbulent shear stress,

τ_{ki}: interfacial shear stress,

g: gravitational acceleration,

$\underline{M}_{ik}$: the sum of interfacial drag and lift force.

The energy equation is represented by

$$\frac{\partial}{\partial t}(\alpha_k \rho_k e_k) + \nabla \cdot (\alpha_k \rho_k e_k \underline{u}_k) = -\nabla \cdot [\alpha_k (q_k + q_k^T)] - P \frac{\partial}{\partial t} \alpha_k - P \nabla \cdot (\alpha_k \underline{u}_k) + \Phi_k^T + \Phi_k^\mu + Q_{ik} + \Gamma_k h_{ki} + \underline{M}_{ik} \cdot (\underline{u}_{ki} - \underline{u}_k) + \nabla \alpha_k \cdot \tau_k \cdot (\underline{u}_{ki} - \underline{u}_k) + q_{wk} \tag{3}$$

where e_k: internal energy of k-phase,

Φ_k^T: turbulent energy source,

Φ_k^μ: viscous dissipation,

Q_{ik}: interfacial heat transfer,

q_{wk}: wall heat flux.

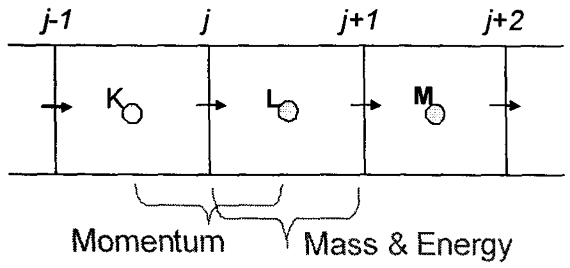

Fig. 2 Staggered grid mesh.

It is assumed that the continuous liquid and entrained liquid are in a thermal equilibrium. Thus, the sum of the two liquid energy equations(the continuous liquid and entrained liquid energy equations) is solved. As a result, five scalar equations(i.e., three continuity and two energy equations) and three momentum equations are used.

The independent state variables for the scalar equations are chosen to be P, α_v, α_d, e_l, and e_v. For each component of the k-phase momentum equations, the corresponding velocity component is regarded as an independent variable.

For a mathematical closure, equations of the states (EOS) and constitutive relations are needed. That is, the thermodynamic variables such as densities, temperatures, etc., are expressed as functions of pressure and phasic internal energy. The saturation property is represented as a function of pressure. All the terms in the right-hand sides of Eqs.(1) through (3), including the interfacial heat, mass, and momentum transfer terms, are also given as functions of the independent state variables and phasic velocities.

3. Numerical Solution Method

The semi-implicit coupled ICE scheme was adopted as a basis of this work. In Section 3.1, the semi-implicit ICE scheme in the RELAP5 code[1] is introduced first for simplicity. The RELAP5 code uses a one-dimensional two-fluid model. It adopts a finite difference method based on a staggered grid. Meanwhile, we use the three-dimensional, three-field model and a finite volume method over an unstructured grid. Thus, some modifications to the numerical scheme are needed. These are explained in Section 3.2.

3.1 The Semi-Implicit ICE Scheme

In the RELAP5 code, the continuity, momentum, and energy equations for liquid and vapor phases are used, which are similar to Eq. (1) through Eq. (3). Because of the one-dimensional approach, the viscous and turbulent shear stress terms in the momentum equations are represented by a wall friction term.

Fig. 2 shows the one-dimensional staggered mesh. At first, the liquid and vapor momentum equations in an expanded form are integrated over the momentum cell j in Fig. 2. The convection term in the momentum equation is explicitly treated, whereas the pressure gradient, interfacial drag, and wall friction terms are implicitly treated. This approach yields two coupled equations with two unknown phasic velocities at junction j and unknown pressures at the adjacent cells. By solving the equations, the new time phasic velocity at junction j is represented as a function of the pressures of the adjacent cells K and L:

$$u_{k,j}^{n+1} = u_{k,j}^{\exp} + \beta_{k,j}(\delta P_K - \delta P_L) \quad (4)$$

where $\delta P = P^{n+1} - P^n$,

n: old time step

n+1: new time step

$u_{k,j}^{\exp}$: new time velocity of k-phase based on the old time pressure gradient,

$\beta_{k,j}$: coefficient derived from the phasic momentum equations.

Next, the mass and energy equations are integrated over a hydrodynamic cell L. In the convection terms of the scalar equations, the convected properties (i.e., $\alpha_k \rho_k$ in the mass equations and $\alpha_k \rho_k e_k$ in the energy equations) are explicitly determined by using the donor-cell scheme and the velocities are implicitly treated. Meanwhile, the interfacial heat and mass transfer terms are implicitly treated, resulting in phase-coupled continuity and energy equations[1]. The resulting discretized equations are ordered in the following sequence: (i) vapor energy equation, (ii) liquid energy equation, (iii) the difference of the phasic continuity equations, and (iv) the sum of the phasic continuity equations. These equations are linearized with respect to four independent state variables, (e_v, e_l, α_v, P). Then they are represented as

$$\underline{\underline{A}}\,\underline{x} = \underline{s} + \underline{g}^1 u_{v,j+1}^{n+1} + \underline{f}^1 u_{l,j+1}^{n+1} + \underline{g}^2 u_{v,j}^{n+1} + \underline{f}^2 u_{l,j}^{n+1} \quad (5)$$

where $\underline{\underline{A}}$: 4x4 matrix obtained from the above-mentioned scalar equations,

$\underline{x}$: solution vector, $\underline{x} = col(\delta e_v, \delta e_l, \delta \alpha_v, \delta P)$,

s, $\underline{g}^1, \underline{f}^1, \underline{g}^2$, and $\underline{f}^2$: coefficient vectors (known).

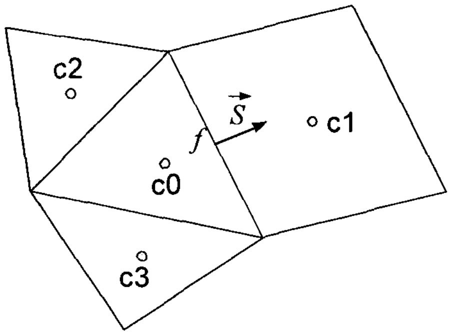

Fig. 3 Control volumes and geometric vector.

Multiplying Eq. (5) by $\underline{\underline{A}}^{-1}$, the bottom row in Eq. (5) results in a single equation involving the pressure and the unknown velocities. Substituting Eq. (4) into this equation yields a single equation involving only the pressures. This is done for each computational cell and, at last, an N x N system of linear equations for the new time pressures in a system containing N cells is established. By solving the system of equations, the new time pressures are obtained, which are substituted into Eq. (4) to obtain the new time velocities. Now, the new time independent variables are obtained from Eq. (5). Finally, a correction step is implemented to correct the errors due to the use of the expanded form of the scalar equations.

3.2 The Unstructured Semi-Implicit ICE Scheme Using a Finite Volume Method

The unstructured mesh is characterized with no continuous grid line in the mesh. And it is constructed by non-overlapping polygonal cells which can be used as a basic element for applying a conservation law expressed in the governing equations of the two-phase flows. Figure 3 shows an example of an unstructured grid with Cartesian coordinates in two dimensions, where c1, c2 and c3 are the neighboring cells of the cell c0, and $\vec{S}$ is the area vector of the face f between the cell c0 and the cell c1.

To apply the semi-implicit ICE scheme to an unstructured grid, it should be modified because the conventional fully staggered-grid method cannot be used and, instead, a non-staggered (cell-centered co-located) scheme is adopted. All the variables except for the phasic volume flow which is defined on each cell face are located at the cell center. But the basic concept such as a coupling among the energy, pressure and volume fraction variations is applicable without any change.

At first, the phasic momentum equations in an expanded form are integrated over the control volume c0 in Fig. 3. The interface momentum transfers such as the drag and virtual mass force in Eq. (2) are calculated implicitly, whereas the other terms are treated explicitly. This results in three coupled phasic momentum equations with three unknown phasic velocities, $\underline{u}_{k,c0}^{\exp}$. Thus the phasic velocity can be represented by

$$\underline{u}_{k,c0}^{\exp} = \underline{S}_{k,c0}^{n} + \beta_{k,c0}\nabla p_{c0}^{n} \tag{6}$$

where $\underline{S}_{k,c0}^{n}$ includes the explicit convection, diffusion, and body force contributions and $\beta_{k,c0}$ is the coefficient of the pressure gradient. The resulting phasic velocity at the cell center does not satisfy a mass conservation because the old time pressure was used. Next, the new time phasic velocities are calculated by considering the pressure gradient term implicitly.

$$\underline{u}_{k,c0}^{n+1} = \underline{S}_{k,c0}^{n} + \beta_{k,c0}\nabla p_{c0}^{n+1} \tag{7}$$

Subtracting Eq. (6) from Eq. (7) we obtain:

$$\underline{u}_{k,c0}^{n+1} = \underline{u}_{k,c0}^{\exp} + \beta_{k,c0}\nabla \delta p_{c0} \tag{8}$$

where $\delta p_{c0}(= p_{c0}^{n+1} - p_{c0}^{n})$ is a pressure correction which will be determined so that the mass conservation is satisfied.

The new time phasic velocity at the cell face f, $\underline{u}_{k,f}^{n+1}$, is needed for the calculation of the convective flux. This is obtained by

$$\underline{u}_{k,f}^{n+1} = \underline{u}_{k,f}^{\exp} + \beta_{k,f}\frac{\delta p_{c1} - \delta p_{c0}}{|d\vec{r}_{01}|}\vec{n} \tag{9}$$

where $\underline{u}_{k,f}^{\exp}$ and $\beta_{k,f}$ are the phasic velocity and coefficient at the cell face f (between the cells c0 and c1), respectively, $\vec{n}$ is an outward face normal vector, and $|d\vec{r}_{01}|$ is the distance between the cell centers of c0 and c1. The phasic velocity at the cell face f, $\underline{u}_{k,f}^{\exp}$, is obtained by interpolating the neighboring cell-center velocities. In order to hinder the well-known checker-boarding phenomena in a pressure field, a 3rd-order pressure damping term is added to the face velocity in the context of the pressure-weighted interpolation method proposed by Rhie and Chow[16]:

$$\underline{u}_{k,f}^{exp} = \xi \underline{u}_{k,c0}^{exp} + (1-\xi)\underline{u}_{k,c1}^{exp} - \beta_{k,f}\left\{\frac{p_{c1}^n - p_{c0}^n}{|d\vec{r}_{01}|}\vec{n} + \xi\nabla p_{c0}^n + (1-\xi)\nabla p_{c1}^n\right\} \quad (10)$$

where ξ is a weighting factor. The cell face coefficient $\beta_{k,f}$ is simply an arithmetic mean of the neighboring cells:

$$\beta_{k,f} = \xi\beta_{k,c0} + (1-\xi)\beta_{k,c1} \quad (11)$$

As a result, the new time phasic velocity at a cell face is represented by Eq. (9) as a function of the pressures of the adjacent cells, which is similar to Eq. (4).

To obtain the convective fluxes in all the scalar equations, the phasic volume flow at each cell face $\Psi_{k,f}^{n+1}$ is needed first. This is obtained by

$$\Psi_{k,f}^{n+1} = \Psi_{k,f}^{exp} + \beta_{k,f}\frac{\delta p_{c1} - \delta p_{c0}}{|d\vec{r}_{01}|}\vec{n}\cdot\vec{S} \quad (12)$$

where $\Psi_{k,f}^{exp} = \underline{u}_{k,f}^{exp}\cdot\vec{S}$ and $\vec{S}$ is the surface vector. Eq. (12) corresponds to Eq. (4) in the staggered-grid scheme.

Thereafter, the five scalar equations are integrated over cell c0. The convected properties are explicitly determined and the phasic volume flow at each cell face is implicitly treated. This process is similar to that in Section 3.1. The resulting discretized equations are ordered in the following sequence: (i) vapor energy equation, (ii) total liquid energy equation, (iii) vapor continuity equation, (iv) entrained liquid continuity equation, and (v) continuous liquid continuity equation. These are linearized with respect to five independent state variables (e_v, e_l, α_v, α_d, P) and rearranged as

$$\underline{\underline{A}}\underline{x} = \underline{s} + \sum_{j=1}^{nb(c0)}\underline{g}\Psi_{v,j}^{n+1} + \sum_{j=1}^{nb(c0)}\underline{f}\Psi_{l,j}^{n+1} + \sum_{j=1}^{nb(c0)}\underline{d}\Psi_{d,j}^{n+1} \quad (13)$$

where $\underline{\underline{A}}$: 5x5 coefficient matrix obtained from the above-mentioned 5 scalar equations,

$\underline{x}$: solution vector,

$\underline{x} = col(\delta e_v, \delta e_l, \delta\alpha_v, \delta\alpha_d, \delta P)$,

s, *g*, *f*, and *d*: coefficient vectors (known),

nb(i): number of the cell faces of cell *i*.

The unknown fluxes in Eq. (13) are substituted with Eq. (12), from which a pressure equation for the cell c0 can be obtained. The remaining numerical sequence is the same as that in Section 3.1. However, in the non-staggered method, the face volume flux along with the cell-centered velocity is updated by using the new time pressure correction. Equations (12) and (8) are applied at this stage. When all the cell-centered variables and face-centered phasic volume flows are updated, the new time solutions are obtained.

4. RESULTS OF PRELIMINARY CALCULATIONS

To examine the unstructured semi-implicit ICE scheme, a one-dimensional pilot code was developed first and numerical tests were conducted. Afterwards, a code using a 3D unstructured grid was developed. In the two codes, the physical models were considerably simplified and will be improved further later. The preliminary results of the two codes are presented in this section. It is noted that the calculations have been done for a verification of the numerical method from a qualitative point of view.

4.1 BOILING FLOW IN A ONE-DIMENSIONAL VERTICAL PIPE

The flow in a vertical pipe of 0.1 m in diameter and 6 m in length was simulated. Initially the pipe was filled with subcooled water. Slightly subcooled water at a temperature of 450.95 K was introduced at a velocity of 4.0 m/s into the inlet. A volumetric heat source was imposed for the whole pipe; it was linearly increased from 0 MW/m^3 to 23.0 MW/m^3 during the first 10 s and then remained constant. The exit pressure was kept constant at 1.0 MPa. This problem was simulated by the one-dimensional pilot code. Equal-length meshes were used for 5 different calculations using 20, 40, 60, 120 and 240 meshes, respectively.

To reach a steady state, a null-transient calculation was carried out for 40s. Fig. 4 shows the volume fraction behaviors of the vapor, continuous liquid, and entrained liquid at the exit. Initially the flow was single-phase liquid flow and, from 5s, it changed into a two-phase flow. At about 17s, the calculation reaches a steady state with a three-field flow. Thus, it can be said that flow transitions are well represented by this numerical scheme. For this calculation, 40 meshes (with 0.15 m/mesh) were used.

Fig. 5 shows the steady-state axial void distributions with different meshes, which clearly illustrate a mesh convergence. The conservations of the mass and energy

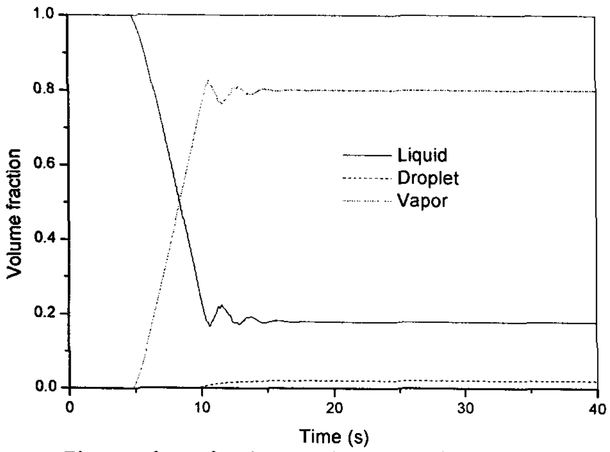

Fig. 4 Volume fraction at exit during null transient.

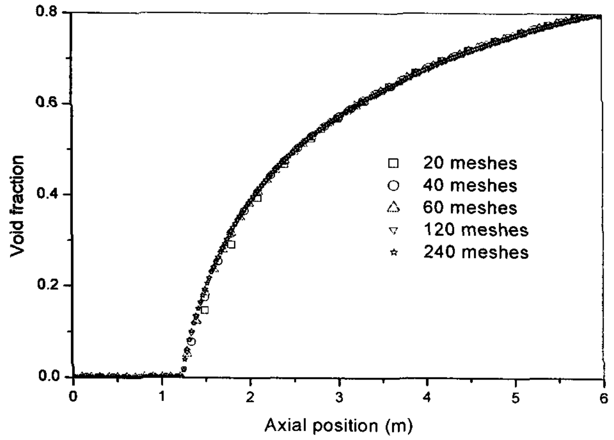

Fig. 5 Steady-state axial void distributions.

were also confirmed by comparing the inlet and exit flow conditions.

4.2 Two-Dimensional Single-Phase Water Flow

To verify the unstructured numerical scheme, a single-phase water flow in an X-Y plane (0.1 m x 0.4 m) was simulated by using a structured grid with 880 rectangular meshes and an unstructured grid with 954 triangular meshes, which are depicted in Fig. 6. The pressures at the inlet (bottom) and the exit (top) were 1,000,020 Pa and 1,000,000 Pa, respectively. The water density was 943.0 kg/m^3 and the viscosity was artificially increased to 0.1 N·s/m^2 to produce a laminar flow.

Initially the flow was stagnant and a null transient calculation was carried out to attain a steady state. Figure 7 shows a comparison of the steady-state Y-direction velocities at y=0.3 m. Two solutions in Fig. 7 are very similar to each other. This clearly shows that the unstructured semi-implicit ICE numerical scheme works

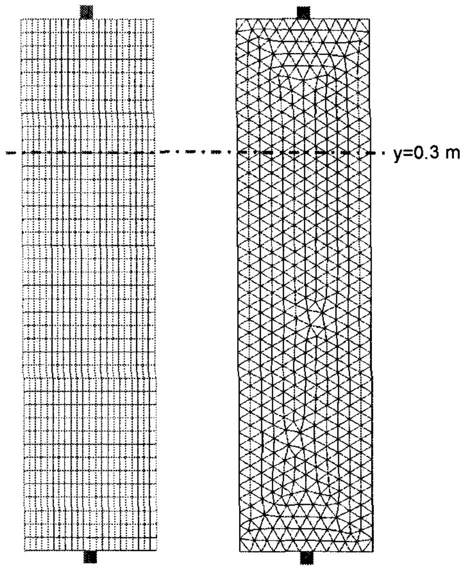

Fig. 6 2D structured and unstructured grids; 880 rectangle and 954 triangle meshes were used, respectively.

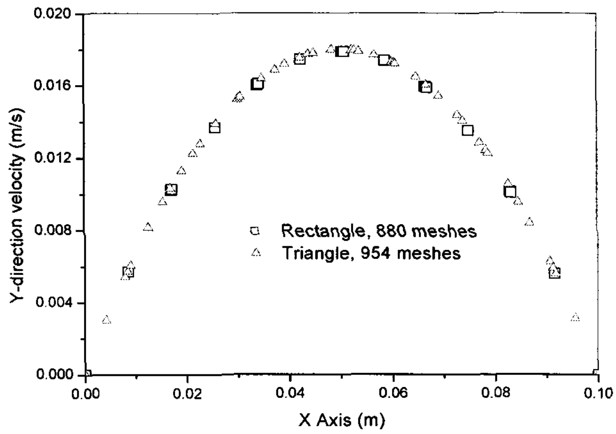

Fig. 7 Comparison of the Y-direction velocities at y=0.3 m.

well for both the structured and unstructured grids.

4.3 Boiling Flow in a Three-Dimensional Vertical Duct

For a verification of the 3D unstructured numerical scheme, boiling in a vertical pipe of 1 m in diameter and 2 m in height was simulated. Figure 8(a) shows the unstructured grid using the Voronoi polygons for the X-Y plane. For the axial direction, 10 equal-length meshes were used. The total number of cells is 1110. A volumetric heat source was given for the whole pipe; linearly increased from 0 MW/m^3 to 20.0 MW/m^3 during the first 10s and then remained constant. Subcooled water was introduced to the inlet at a constant velocity of 0.1 m/s. The exit pressure was maintained at 1.0 MPa.

Fig. 8(b) and (c) show the steady state results at 25s;

the void fraction and the vapor-phase velocity fields due to a boiling were predicted well. The conservation of the mass was also confirmed as shown in Fig. 9. The mass flow difference in Fig. 9 is defined as the mass flow rate difference at the exit and the inlet divided by the inlet mass flow rate. At a steady-state flow, the mass flow difference should be zero. At the beginning of the transient, it was nearly zero and, at about 6s, increased a lot because the exit flow rate suddenly increased due to a boiling in the duct. However, at last, the mass flow difference becomes below 10^{-4} %. The results of this calculation show that the semi-implicit ICE algorithm based on the unstructured grid works well qualitatively and the mass is conserved.

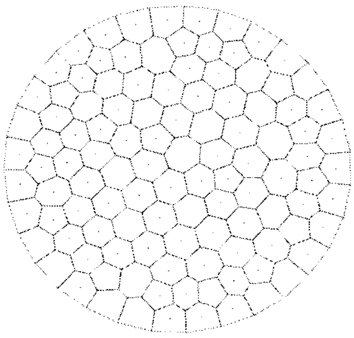

(a) Top view of the unstructured grid

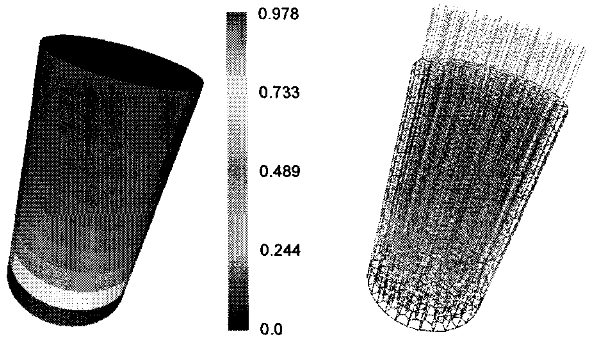

(b) Void fraction (c) Vapor-phase velocity

Fig. 8 The unstructured grid and the results of calculations.

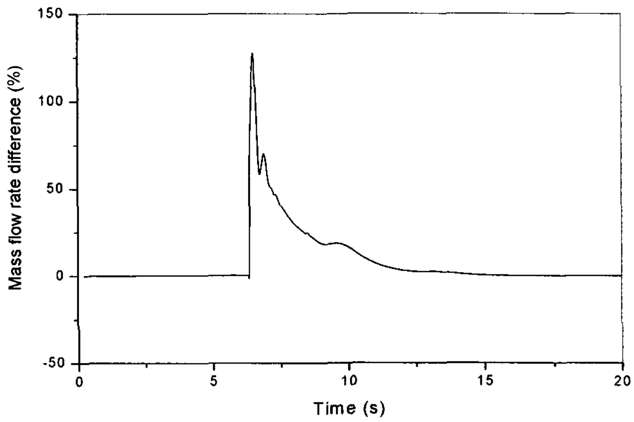

Fig. 9 Behavior of the mass flow difference, $(\dot{m}_{exit} - \dot{m}_{inlet})/\dot{m}_{inlet}$.

4.4 Flashing in a Horizontal Pipe

A flashing is an important physical phenomenon in a nuclear system or a component analysis. To assess the developed code's capability to predict a flashing, a conceptual problem was established. A 2-dimensional plane of 0.1 m x 2 m was considered. This plane is modeled with 250 rectangular cells as shown in Fig. 10(a). Each mesh is 0.02m x 0.04m. The left and the right ends were designated as the inlet and the exit, respectively. The inlet velocity was kept constant at 4.0 m/s. The inlet water temperature was 450.0 K. The exit pressure was linearly decreased as a function of the time during the first 10s from 1.0 MPa to 0.854 MPa, and then, remained constant. The saturation temperatures at 1.0 MPa and 0.854 MPa are 453.034 K and 446.270 K, respectively. Therefore the flow was initially subcooled, but a two-phase flow is expected later due to a flashing.

During the first 10s, the flow in the 2D plane experienced transitions from a single-phase water to a two-phase mixture flow by a flashing. This transient process was predicted well. At 13s, the calculation reached a steady state. Fig. 10(b) through 10(e) show the pressure, void, and x-direction liquid and vapor phase velocities at 13s, respectively. The inlet pressure was predicted to be 0.88 MPa when the pressure at the exit was given at 0.854 MPa. This means the superheated water is injected into the inlet since the saturation temperature at 0.88 MPa (i.e. 447.55K) is lower than the inlet temperature. Both the void fraction and velocity increase along the flow path to the exit because a flashing occurs over the entire region. In all the computational cells, the liquid was slightly superheated and the steam was nearly saturated. These results are physically reasonable.

This problem was simulated again by using a one-dimensional system code, MARS[4]. An input model with 20 equal-length meshes was used for the MARS calculation and the same boundary conditions were specified. The results were very similar to each other. In the 2D calculation, the steady-state void fraction at the exit was 0.604, whereas it was 0.585 in the MARS calculation. This difference is due to the differences in the geometry input model and the interfacial drag model that

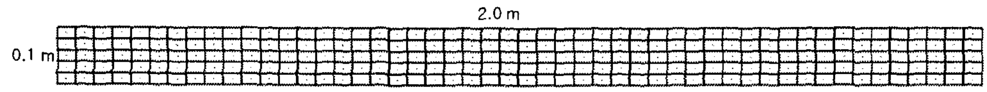

(a) Calculation mesh

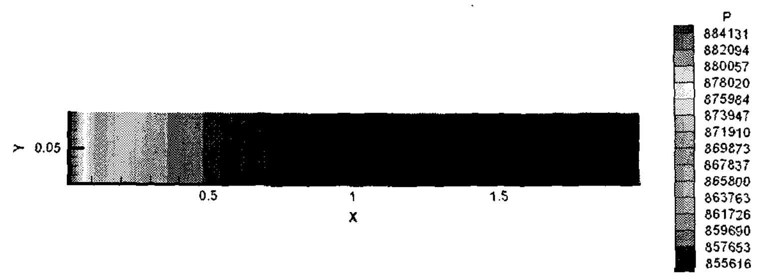

(b) Pressure distribution

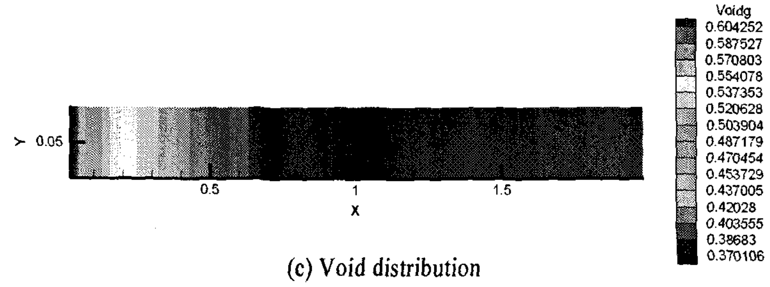

(c) Void distribution

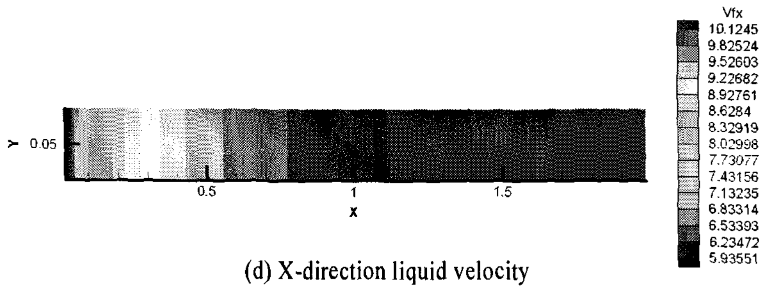

(d) X-direction liquid velocity

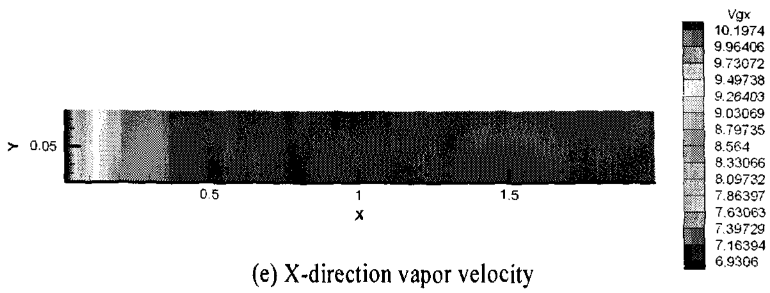

(e) X-direction vapor velocity

Fig. 10 Calculation of the flashing in a horizontal pipe using a 2D grid.

strongly affects the relative velocity and, in turn, void fraction.

4.5 Cavitation with a Sudden Contraction

A cavitation with a sudden contraction was simulated by using a 2D structured grid. Figure 11(a) shows the 2D grid for this problem. The entire volume was modeled with 600 cells with a size of 0.01m x 0.01m. The left and the right ends were designated as the inlet and the exit, respectively. The water velocity at the inlet was 3.0 m/s and the pressure at the exit was 1.0 MPa. The inlet water temperature is 453.0 K, which is slightly lower than

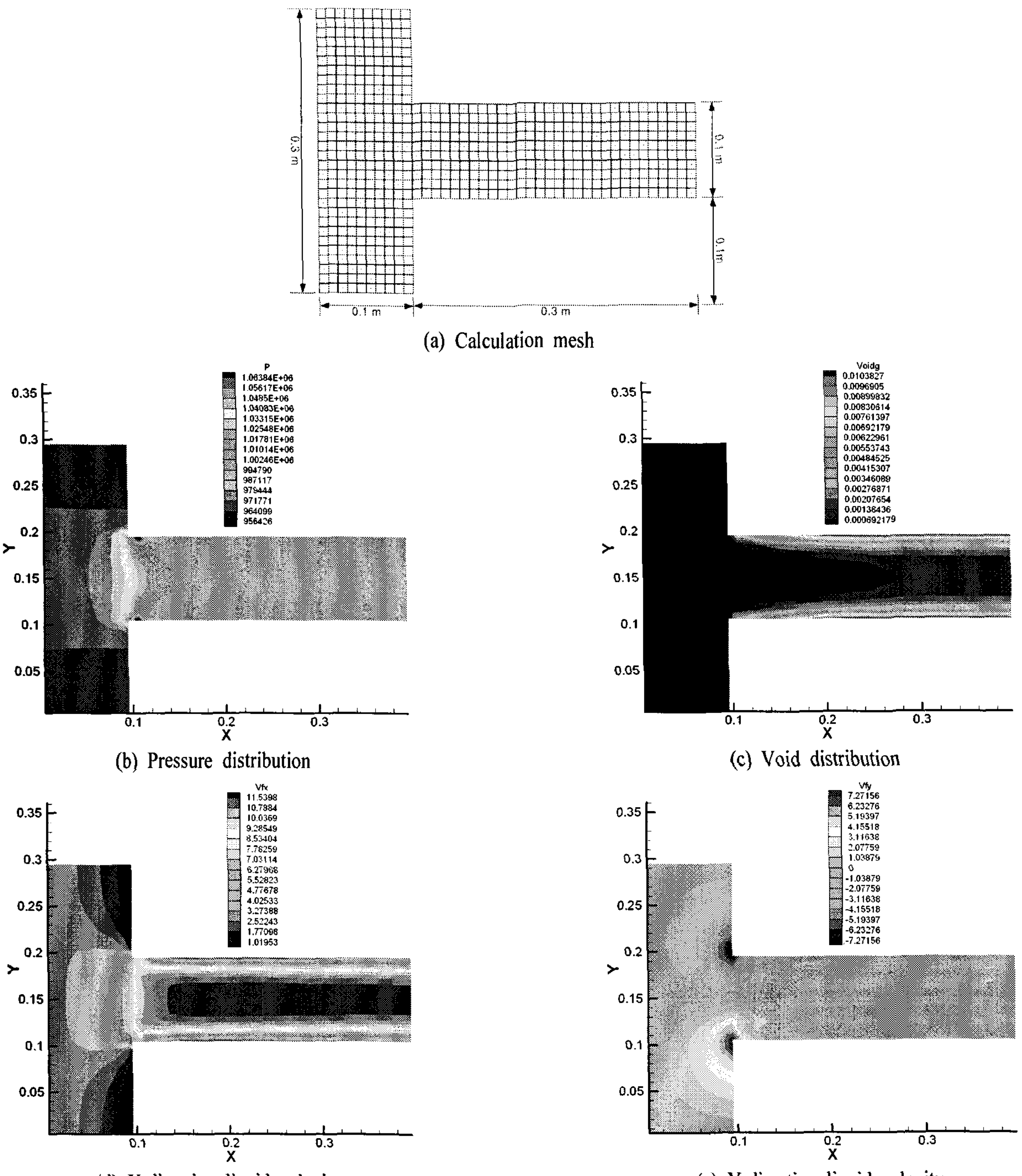

(a) Calculation mesh

(b) Pressure distribution

(c) Void distribution

(d) X-direction liquid velocity

(e) Y-direction liquid velocity

Fig. 11 Calculation of the cavitation with a sudden contraction using a 2D grid.

the saturation temperature at 1.0 MPa (i.e., 453.034 K).

Fig. 11(b) through 11(e) show the steady-state results. As can be seen in Figs. 11(d) and 11(e), the flow is accelerated at a sudden contraction. Thus, the pressure near the walls close to the throat decreases to 0.96 MPa, which is lower than the exit pressure. The temperatures in these areas are higher than the saturation temperature. This results in a local cavitation, and thus, steam generates near the walls. The maximum void fraction was predicted to be about 0.01. These results are also physically reasonable.

5. CONCLUSIONS

A 3D hydrodynamic solver for a transient two-fluid three-field model has been developed, which is based on an unstructured non-staggered grid. For the numerical solution scheme of the solver, the semi-implicit ICE scheme was applied for an unstructured grid. To examine the unstructured semi-implicit ICE scheme, one-dimensional and three-dimensional pilot codes were developed. These were verified against a few conceptual problems. The test calculations were carried out for both structured and unstructured grids including 1D, 2D, and 3D grids. The results show that the numerical scheme is applicable for the prediction of phase changes and flow transitions due to a boiling and a flashing. The strong coupling between the pressure and void fraction changes was predicted well. The conservations of the mass and energy were also verified. Thus, it is believed that the unstructured semi-implicit ICE scheme can be utilized as a hydrodynamic solver for the 3D component of a system code and component-scale analysis tools.

Qualitative assessments against complicated 3D two-phase flows are going to be conducted soon. Thereafter, physical models including a turbulence model will be implemented and a systematic validation will be carried out. Of course, further improvements to the developed numerical scheme are also necessary for an enhanced accuracy and computational efficiency.

ACKNOWLEDGEMENT

This work has been performed as a part of the Nuclear Research and Development Program supported by the Ministry of Science and Technology of the Republic of Korea.

REFERENCES

[1] 2001, The RELAP5-3D Code Development Team, "RELAP5-3D Code Manual Volume I: Code Structure, System Models and Solution Methods," *Idaho National Engineering and Environmental Laboratory.*

[2] 1993, Spore, J.W., et al., "TRAC-PF1/MOD2 Volume I. Theory Manual, NUREG/CR-673", *Los Alamos National Lab.*

[3] 1996, Bestion, D., Barre, F. and Faydide, F., "Methodology, Status and plans for development and assessment of CATHARE code," *OECD/CSNI Workshop on Transient Thermal-Hydraulic & Neutronic Codes Requirements*, Nov.5-8.

[4] 1999, Jeong, J.J., et al., "Development of a multi-dimensional thermal-hydraulic system code, MARS 1.3.1," *Annals of Nuclear Energy*, Vol.26, No.18, pp.1611-1642.

[5] 1996, Kelly, J.M., "Thermal-hydraulic modeling needs for passive reactors," *OECD/CSNI Workshop on Transient Thermal- Hydraulic & Neutronic Codes Requirements*, Nov.5-8.

[6] 2000, Toumi, I., et al., "FLICA-4: a three-dimensional two-phase flow computer code with advanced numerical methods for nuclear applications," *Nucl. Eng. Design*, Vol.200, pp.139-155.

[7] 1982, Singhal, A.K., et al., "ATHOS - A Computer Program for Thermal-Hydraulic Analysis of Steam Generators, Volume 1: Mathematical and Physical Models and Method of Solution," *Electric Power Research Institute.*

[8] 2001, Goerge, T.L., et al., "GOTHIC Containment Analysis Package Technical Manual, Ver.6.1b," *Electric Power Research Institute.*

[9] 2003, Yadigaroglu, G., Andreani, M., Dreier, J. and Coddington, P., "Trends and needs in experimentation and numerical simulation for LWR Safety," *Nucl. Eng. Design*, Vol.221, pp.205-223.

[10] 2007, Bieder, U. and Graffard, E., "Qualification of the CFD code Trio-U for full scale reactor applications," *Nucl. Eng. Design*, doi:10.1016/j.nucengdes.2007.02.040.

[11] 2005, Yadigaroglu, G., "Computational fluid dynamics for nuclear applications: from CFD to multi-scale CMFD," *Nucl. Eng. Design*, Vol.235, pp.153-164.

[12] 2007, Guelfi, A., et al., "NEPTUNE, a new software platform for advanced nuclear thermal hydraulics," *Nucl. Sci. Eng.*, Vol.156, pp.281-324.

[13] 1975, Harlow, F.H. and Amsden, A.A., "Numerical calculation of multiphase fluid flow," *J. Computational Physics*, Vol.17, p.19.

[14] 1978, Liles, D.R. and Reed, W.H., "A semi-implicit method for two-phase fluid dynamics," *J. Computational Physics*, Vol.26, pp.390-407.

[15] 2006, Ishii, M. and Hibiki, T., "Thermo-fluid Dynamics of Two-Phase Flow," *Springer*, pp.155-169.

[16] 1983, Rhie, C.M. and Chow, W.L., "Numerical study of the turbulent flow past an airfoil with trailing edge separation," *AIAA Journal*, Vol.21. No.11, pp.1525-1532.